# Correction of misalignment errors in the magnetic gradient tensor measurement system and its application in localization

Yali Shen<sup>1,2</sup>, Yingzi Zhang<sup>1,2\*</sup>, and Qingping Yang<sup>3</sup>

**Abstract.** The magnetic gradient tensor measurement system (MGTMS) is critical for detecting and localizing ferromagnetic targets. However, its localization accuracy is closely linked to measurement precision, which is often compromised by sensor misalignment errors. To mitigate these errors, this study proposes a practical calibration method using a standard magnetic source, achieving effective misalignment correction with minimal system alteration. The proposed method is validated through both simulations and localization experiments. Simulation results indicate that the root mean square error (RMSE) of the calibrated tensor values is reduced by three orders of magnitude compared to the uncalibrated state. Experimental results further demonstrate that the average localization error decreases from 0.040 m to 0.019 m after calibration, corresponding to a 52.5% improvement in positioning accuracy. These results highlight the potential of improving the accuracy of MGTMS-based target localization in practical applications.

#### 1 Introduction

Magnetic anomaly detection has received widespread attention due to its effectiveness in locating small magnetic targets in both underground and underwater environments [1]-[3]. Many existing localization algorithms, such as Scalar Triangulation and Ranging (STAR)[4], Nara method [5], Normalized Source Strength (NSM)[6] and the New Two-Point Tensor (NTPT) approach [7], rely heavily on magnetic gradient tensor (MGT) information. However, the localization accuracy of these methods is significantly affected by array misalignment errors in the magnetic gradient tensor measurement system (MGTMS)[8][9].

To enhance localization precision, various error correction methods have been proposed. For instance, Y. Mu et al. utilized magnetic gradient tensor invariants under non-uniform background fields to correct misalignment errors<sup>[10]</sup>. C. Chi et al. introduced a total least squares (TLS)-based calibration method tailored to MGTMS error sources[11]. X. Zhang et al. further developed a two-stage approach combining TLS ellipsoid truncation with differential evolution (DE) optimization to sequentially correct sensor-intrinsic and alignment-related errors<sup>[9]</sup>. Additionally, C. Li et al. proposed a tensor error compensation strategy based on damped Levenberg-Marquardt  $(DA_LM)$ algorithm<sup>[12]</sup>. Most of these methods estimate misalignment errors by rotating the MGTMS and measuring tensor values at multiple orientations, assuming that the theoretical gradient tensor should

vanish in a magnetically quiet environment. However, due to the typically large size of

MGTMS platforms, physical rotation is often impractical. Moreover, during the rotation process, sensor positions may shift due to cable tension, thereby introducing additional errors and compromising the accuracy of misalignment angle estimation.

Therefore, this study presents a novel non-contact calibration method that involves placing the MGTMS in an environment with minimal external magnetic interference and recording tensor measurements of the standard magnetic source at multiple positions. Through analytical derivation of theoretical tensor values at distinct locations followed by Particle Swarm Optimization (PSO)-based residual minimization between measured and theoretical tensors, the misalignment error is precisely determined. The proposed method obviates system movement by substituting the pose adjustment of the MGTMS with directional changes of the standard magnetic source, thus transforming the estimation of calibration parameters as a process based on multiple source positions. Consequently, the quadratic errors induced by system motion are effectively mitigated.

# 2 Modeling of Rotation Misalignment Error and Magnetic Gradient Tensor Correction

When the distance between the standard magnetic source and the observation point exceeds 2.5 times the

<sup>&</sup>lt;sup>1</sup>North University of China, State key Laboratory of Extreme Environment optoelectronic Dynamic Testing Technology and Instrument, 030051 No. 3 Xueyuan Road, Jiancaoping, Taiyuan, China

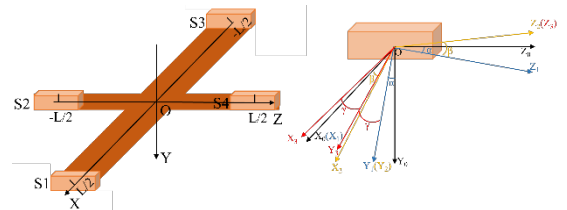
<sup>&</sup>lt;sup>2</sup>North University of China, School of Instrumentation and Electronics, 030051 No. 3 Xueyuan Road, Jiancaoping, Taiyuan, China <sup>3</sup>Brunel University of London, Department of Mechanical and Aerospace Engineering, Kingston lane, Uxbridge UB8 3PH, UK

<sup>\*</sup> Corresponding author: <u>zhangyingzi@nuc.edu.cn</u>

size of the standard magnetic source itself, the standard magnetic source can be effectively modeled as a magnetic dipole<sup>[13]</sup>. In this study, the standard magnetic source is treated as a magnetic dipole and can be expressed as:

$$\boldsymbol{B} = \frac{\mu_0}{4\pi} \frac{3(M \cdot r)r - MR^2}{R^5} \tag{1}$$

 $\boldsymbol{B} = \frac{\mu_0}{4\pi} \frac{3(\boldsymbol{M} \cdot \boldsymbol{r}) \boldsymbol{r} - \boldsymbol{M} R^2}{R^5}$  (1) where  $\boldsymbol{B}$  represents the magnitude of the magnetic dipole field,  $\mu_0$  denotes the vacuum permeability, and  $M = [m_x, m_y, m_z]^T$  represents the three components of the magnetic moment of the dipole. The vector  $\mathbf{r} = [x, y, z]^T$ indicates the relative position vector from the magnetic sensor to the magnetic dipole, while *R* is the magnitude



(a) Cross shaped magnetometer array. (b) Schematic diagram of coordinate system conversion for sensor misalignment error.

Fig. 1. Cross shaped MGTMS schematic diagram.

As illustrated in Fig. 1(a), the cross-shaped MGTMS consists of four triaxial magnetic sensors (S1-S4) arranged in an orthogonal baseline configuration with a defined baseline length L in a three-dimensional Cartesian coordinate system. Due to technological limitations during assembly, the system is susceptible to both displacement and rotational misalignment errors. While displacement errors can be effectively reduced through high-precision manufacturing, rotational misalignment remains more difficult to eliminate.

For each sensor Si (i=1,2,3,4), the measured magnetic field vector is denoted as  $\mathbf{B}_i = [B_{ix}, B_{iy}, B_{iz}]^T$ , representing the three orthogonal components of the magnetic field along the x-, y-, and z-axes, respectively.

Due to rotational misalignment errors, the coordinate systems of each sensor deviate from the reference coordinate system. This deviation results in an inaccurate projection of the measured magnetic field components, ultimately causing the tensor matrix computed from differential calculations to diverge from the true values. Therefore, it is essential to establish the quantitative relationship between the actual coordinate system and the reference coordinate system to correct these misalignment errors. As illustrated in Figure 1(b), the conversion between the standard sensor coordinate system  $(O-X_0Y_0Z_0)$  and the actual sensor coordinate system  $(O-X_3Y_3Z_3)$  can be described by three sequential rotations: first, a rotation of the roll angle  $\alpha$  around the  $X_0$  axis; second, a rotation of the pitch angle  $\beta$  around the newly generated Y<sub>1</sub> axis; and third, a rotation of the yaw angle  $\gamma$  around the newly generated  $Z_2$  axis. The corresponding transformation matrix for the coordinate

$$R = R_{\gamma}R_{\beta}R_{\alpha}$$

$$= \begin{bmatrix} \cos \gamma & -\sin \gamma & 0 \\ \sin \gamma & \cos \gamma & 0 \\ 0 & 0 & 1 \end{bmatrix} \begin{bmatrix} \cos \beta & 0 & -\sin \beta \\ 0 & 1 & 0 \\ \sin \beta & 0 & \cos \beta \end{bmatrix} \begin{bmatrix} 1 & 0 & 0 \\ 0 & \cos \alpha & -\sin \alpha \\ 0 & \sin \alpha & \cos \alpha \end{bmatrix}$$
(2

According to Equation (2), the magnetic field in a misaligned orthogonal coordinate system can be transformed. The transformation relationship can be expressed as follows:

$$B_{meas} = RB_{ideal} \tag{3}$$

where  $B_{meas}$  represents the actual magnetic field value, while  $B_{ideal}$  denotes the ideal value. Write the expression for  $\mathbf{B}_{ideal}$  according to Equation (3) as follows:

where 
$$S = R^{-1}$$
. (4)

The measurement point of the cross-shaped MGTMS is defined as the geometric center O of the sensor array. According to Maxwell's equations, the divergence and curl of the magnetic field vector B are equal to zero in a passive, static magnetic field. These constraints imply that the magnetic gradient tensor matrix G, defined as the spatial derivative of B, is symmetric and traceless. As a result, only five independent components of G are required to fully characterize the tensor. Based on the cross-shaped array configuration, the magnetic gradient tensor can be approximated using central differences of the measured magnetic field components, as follows:

agnetic field components, as follows:  

$$\mathbf{G} = \begin{bmatrix} G_{xx} & G_{xy} & G_{xz} \\ G_{yx} & G_{yy} & G_{yz} \\ G_{zx} & G_{zy} & G_{zz} \end{bmatrix}$$

$$= \frac{1}{L} \begin{bmatrix} B_{1x} - B_{3x} & B_{1y} - B_{3y} & B_{4x} - B_{2x} \\ B_{1y} - B_{3y} & -(B_{1x} - B_{3x}) - (B_{4z} - B_{2z}) & B_{4y} - B_{2y} \\ B_{1z} - B_{3z} & B_{4y} - B_{2y} & B_{4z} - B_{2z} \end{bmatrix}$$
(5)

where  $B_{ij}$  (i=1,2,3,4; j=x, y, z) represents the jcomponent of the magnetic field value measured by sensor  $S_i$ . Based on the formulas presented above, we can derive the influence of the rotation of the sensor coordinate system on differential magnetic field measurements:

$$\Delta \boldsymbol{B}_{ij}^{cr} = \boldsymbol{B}_{i}^{ideal} - \boldsymbol{B}_{j}^{ideal} = \boldsymbol{S}_{i} \boldsymbol{B}_{i}^{meas} - \boldsymbol{S}_{j} \boldsymbol{B}_{j}^{meas} \qquad (6)$$

$$\Delta \boldsymbol{B}_{ij}^{cr} \quad (i, j=1,2,3,4) \quad \text{represents the differential}$$
magnetic field value between  $Si$  and  $Sj$  after calibration.
$$\boldsymbol{B}_{i(j)}^{ideal} \quad \text{denotes the ideal magnetic field value of } Si(j).$$

Additionally,  $\mathbf{S}_{i(j)} = \left(\mathbf{R}_{\gamma_{i(j)}}\mathbf{R}_{\beta_{i(j)}}\mathbf{R}_{\alpha_{i(j)}}\right)^{-1}$  signifies the inverse of the coordinate system transformation matrix of Si(j), where  $\alpha_{i(j)}$ ,  $\beta_{i(j)}$  and  $\gamma_{i(j)}$  represent the roll angle, pitch angle, and yaw angle of Si(j), respectively. Furthermore,  $B_{i(j)}^{meas}$  indicates the measured magnetic field value of Si(j). Given that G is symmetric and traceless, i.e.  $G_{xy}^{cr} = G_{yx}^{cr}$ ,  $G_{xz}^{cr} = G_{zx}^{cr}$ , and  $G_{yz}^{cr} = G_{zy}^{cr}$ , we can derive the expression for the corrected magnetic gradient tensor matrix as follows:

$$G_{cr} = \begin{bmatrix} G_{xx}^{cr} & G_{xy}^{cr} & G_{xz}^{cr} \\ G_{yx}^{cr} & G_{yy}^{cr} & G_{yz}^{cr} \\ G_{yx}^{cr} & G_{yy}^{cr} & G_{yz}^{cr} \end{bmatrix}$$

$$= \frac{1}{L} \begin{bmatrix} (\Delta B_{13}^{cr})_x & (\Delta B_{13}^{cr})_y & (\Delta B_{13}^{cr})_z \\ (\Delta B_{13}^{cr})_y & -(\Delta B_{13}^{cr})_x - (\Delta B_{42}^{cr})_z & (\Delta B_{42}^{cr})_y \\ (\Delta B_{13}^{cr})_z & (\Delta B_{42}^{cr})_y & (\Delta B_{42}^{cr})_z \end{bmatrix}$$
(7)

where  $G_{cr}$  represents the corrected tensor value.

When the corrected magnetic gradient tensor value approaches the ideal tensor value asymptotically, the corresponding parameter is the one we seek. Therefore, the objective function is defined as follows:

$$f = min \frac{1}{n} \sum_{i=1}^{n} \left[ (G_{xx}^{cr} - G_{xx}^{i})^{2} + (G_{xy}^{cr} - G_{xy}^{i})^{2} + (G_{xz}^{cr} - G_{xz}^{i})^{2} + (G_{yy}^{cr} - G_{yy}^{i})^{2} + (G_{yz}^{cr} - G_{yz}^{i})^{2} \right]$$
(8) where *n* represents the number of measurement

where n represents the number of measurement positions,  $G_{ideal}$  denotes the ideal tensor value, which can be calculated using formulas (1) and (5).

### 3 PSO-based correction method

According to the theoretical derivation presented in Section 2, the calibration method for MGTMS can be formulated as a nonlinear optimization problem. To ensure real-time and accurate calibration, the chosen algorithm should be straightforward and practical, while also demonstrating high accuracy and convergence. Consequently, this study selects the PSO algorithm. The algorithm primarily involves initializing the particle swarm, evaluating fitness values, updating individual best positions, updating population best positions, adjusting particle velocity and position, iterating the process, and ultimately outputting the optimal solution<sup>[14]</sup>.

When initializing the particle swarm, set the population size n to 1000 and the particle dimension to 12. Specifically, the i-th particle contains position information  $x_i = [\alpha_I, \alpha_2, \alpha_3, \alpha_4, \beta_I, \beta_2, \beta_3, \beta_4, \gamma_I, \gamma_2, \gamma_3, \gamma_4]$ , where  $\alpha$ ,  $\beta$ , and  $\gamma$  respectively represent the roll angle, pitch angle, and rotation angle corresponding to the four sensors, respectively, for i=1, 2, 3... 1000. The position range is set to [-1,1], and the speed range is set to [-0.1, 0.1]. The maximum number of iterations is T=1000, with learning factors  $c_1=c_2=1.5$ , and an initial inertia weight of  $\omega=1.0$ , which is updated according to  $\omega=\omega-1/T$ . The particle positions and velocities are randomly initialized within the specified ranges.

The objective function value of the particles is calculated using Equation (8). A smaller objective function value indicates better performance.  $P_i = (p_{il}, p_{i2}, ..., p_{il2})$  is the historical optimal position of the i-th particle. The individual optimal position is updated using the following equation:

$$p_i(t+1) = \begin{cases} p_i(t), & \text{if } f(x_i(t+1)) \ge f(p_i(t)) \\ x_i(t+1), & \text{if } f(x_i(t+1)) < f(p_i(t)) \end{cases}$$
(9)  
In Equation (9),  $t$  represents the number of iterations.

In Equation (9), t represents the number of iterations. The global optimal position g(t) is defined as the best position among the states currently experienced by all particles in the population.

$$g(t) = \min \{ f(p_1(t)), f(p_2(t)), \dots, f(p_n(t)) \}$$
 (10)

The velocity and position of the particles according to the following equation:

$$v_i(t+1) = \omega \cdot v_i(t) + c_1 \cdot rand \cdot (p_i - x_i(t))$$

$$+c_2 \cdot rand \cdot (g_i - x_i(t))$$

$$x_i(t+1) = x_i(t) + v_i(t+1)$$
(12)

In Equations (11) and (12), rand represents a uniform random number within the range of [0,1]. The iterations is repeated T times, with g returned at the end of the iteration to obtain the misalignment error angle.

At this stage, the angle of the misalignment error that needs to be determined has been obtained. According to Equations (2) to (4), the rotation matrix S can be formulated, which can be utilized to correct the data output from the MGTMS.

## 4 Simulation

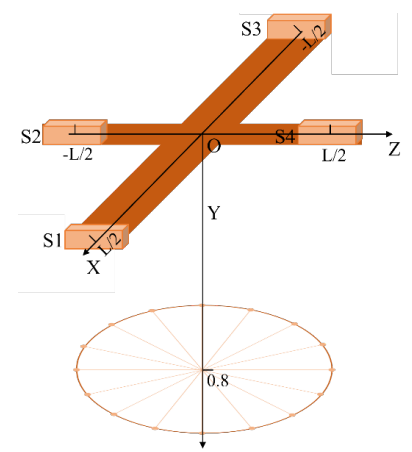


Fig. 2. Closed motion trajectory of standard magnetic source.

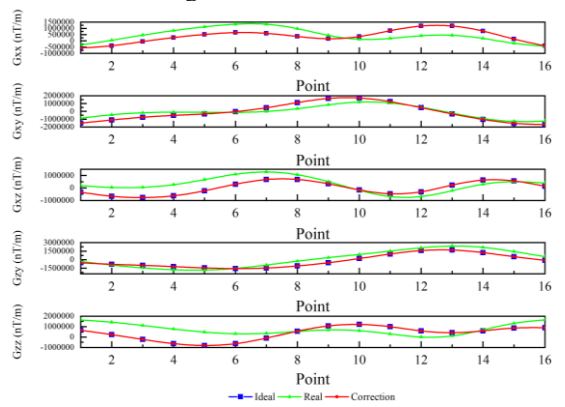
To evaluate the robustness of the proposed method, a closed-loop trajectory simulation model based on magnetic dipole theory was developed, as shown in Figure 2. In this model, a magnetic dipole traverses a circular path with a radius of 0.5 m, and its magnetic moment vector is defined as  $\mathbf{M} = (1200, -3160, 1980)$ A·m<sup>2</sup>. The cross-shaped sensor array has a baseline length of 0.5 m. Sixteen sampling points are uniformly distributed along the trajectory, and the theoretical values of the magnetic gradient tensor (MGT) are computed for all sampling points. The misalignment error parameters introduced into the simulation are listed in Table 1, covering roll ( $\alpha$ ), pitch ( $\beta$ ), and yaw ( $\gamma$ ) angles for each of the four triaxial sensors. These angular errors are integrated into the simulation using Equation (3), and the corresponding measured MGT values are obtained through Equation (7), reflecting the influence of misalignment.

Table 1. Misalignment error of magnetometer.

|       | S1     | S2     | S3     | S4     |
|-------|--------|--------|--------|--------|
| α/rad | 0.448  | -0.227 | 0.634  | -0.556 |
| β/rad | 0.229  | 0.159  | -0.361 | -0.635 |
| γ/rad | -0.132 | 0.554  | 0.336  | 0.632  |

The actual measured magnetic field value is calculated using Equation (3), accounting for misalignment error. Subsequently, the actual measured tensor value is determined from Equation (7).

The PSO algorithm was implemented to compensate for the misalignment errors. The experimental results are illustrated in Figure 3.



**Fig. 3.** Comparison of Tensor Values Before and After Correction.

To correct the misalignment errors, a PSO algorithm was implemented. The calibration results are presented in Figure 3, which compares tensor values before and after calibration. After applying the PSO-based calibration framework, the root mean square error (RMSE) of each MGT component was significantly reduced by nearly three orders of magnitude demonstrating the method's effectiveness. The error reduction metrics are summarized as follows: Gxx decreased from 540,904.089 nT/m to 262.277 nT/m; 464,905.139 nT/m Gxy decreased from 153.131 nT/m; Gxz was reduced from 545,828.167 nT/m to 302.564 nT/m; Gzy decreased from 617,190.071 nT/m to 176.920 nT/m; and Gzz declined from 834,086.836 nT/m to 290.465 nT/m. These results demonstrate the method's efficacy in suppressing sensor misalignment errors and improving MGT measurement accuracy.

# 5 Experiment

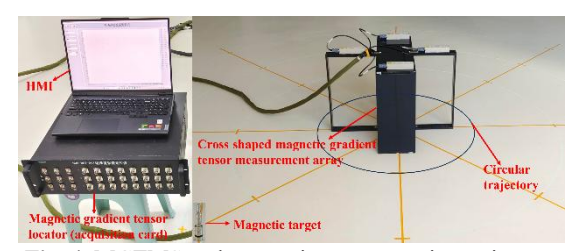
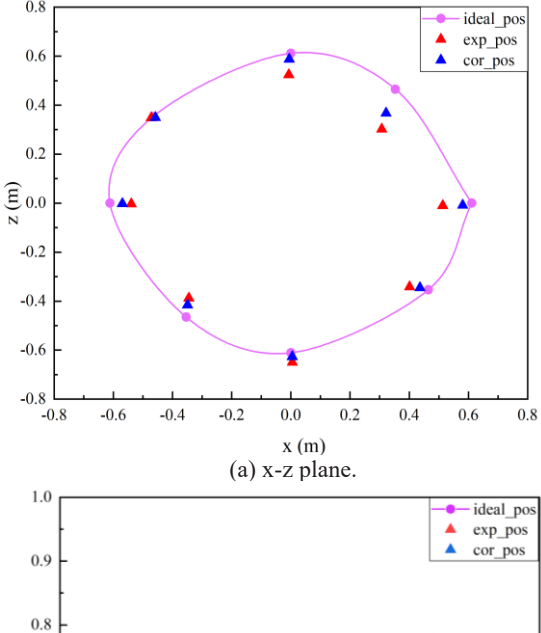


**Fig. 4.** MGTMS and magnetic source motion trajectory diagram.

To further verify the practical efficacy of the proposed correction method, a magnetic source localization experiment was performed using a crossshaped magnetic gradient tensor (MGT) measurement system and a certified reference source. A neodymiumiron-boron permanent magnet, calibrated by the Beijing of Microelectronics Institute Technology possessing a magnetic moment of (0, -1590.29, 0) A·m<sup>2</sup>, was employed as the standard magnetic source. As shown in Figure 4, the sensor array was positioned 0.7 m above the ground, and a circular trajectory with a radius of 0.5 m was marked on the ground, centered at the array's geometric center. Eight sampling points were taken at 45° intervals along the trajectory, and magnetic gradient tensor values were measured at each location.

The NTPT localization algorithm was used to estimate the position of the magnetic source based on the measured tensor values. Three types of localization results were computed for comparison: positions derived from the ideal theoretical tensor, from the uncorrected measured tensor, and from the corrected tensor using the proposed method. Figure 5 shows the localization trajectories obtained from different sources of tensor data. As illustrated, the localization results using the corrected tensor data closely align with the ideal trajectory, in contrast to the more dispersed estimates derived from uncorrected measurements. Table 2 presents the corresponding numerical values. A quantitative comparison reveals that, prior to calibration, the maximum positioning errors along the x-, y-, and zaxes were 0.098 m, 0.048 m, and 0.163 m, respectively. After calibration, these errors decreased to 0.041 m,

0.027 m, and 0.097 m. The average localization error was reduced from 0.040 m to 0.019 m, achieving an improvement of approximately 52.5%.



0.9
0.8
0.6
0.5
0.4
0 1 2 3 4 5 6 7 8 9

Measurement point
(b) y-axis.

**Fig. 5.** Localization results on the trajectory of magnetic source motion.

 Table 2. Localization results on the trajectory of magnetic source motion.

|   | Ideal_position          | Measurement_position    | Correction position     |
|---|-------------------------|-------------------------|-------------------------|
| 1 | (0.611,0.733,0)         | (0.513,0.685,-0.010)    | (0.58, 0.716, -0.008)   |
| 2 | (0.354, 0.733, 0.465)   | (0.307, 0.764, 0.302)   | (0.322, 0.741, 0.368)   |
| 3 | (0, 0.733, 0.611)       | (-0.007, 0.706, 0.524)  | (-0.005, 0.706, 0.587)  |
| 4 | (-0.465, 0.733, 0.354)  | (-0.472,0.703,0.349)    | (-0.458, 0.715, 0.350)  |
| 5 | (-0.611,0.733,0)        | (-0.539,0.774,-0.003)   | (-0.570,0.733,-0.002)   |
| 6 | (-0.354, 0.733, -0.465) | (-0.345, 0.748, -0.388) | (-0.349, 0.736, -0.416) |
| 7 | (0, 0.733,-0.611)       | (0.005, 0.776, -0.650)  | (0.005, 0.745, -0.627)  |
| 8 | (0.465, 0.733, -0.354)  | (0.401, 0.758, -0.342)  | (0.436, 0.726, -0.346)  |

These experimental results are consistent with the simulation findings and demonstrate that the proposed PSO-based calibration method simultaneously addresses correcting tensor distortion and improving the accuracy of MGT-based target localization under practical conditions.

#### 6 Conclusion

This paper proposes a computationally efficient correction method for correcting misalignment errors in MGTMS. By employing a standard magnetic source with a known magnetic moment and utilizing a PSO algorithm, the proposed approach eliminates the need for physically rotating the sensor array, thereby avoiding additional errors caused by structural disturbances or cable tension. Instead, calibration is achieved by

repositioning the magnetic source and comparing the measured and theoretical tensor values at multiple locations. Simulation results demonstrate that the proposed method reduces the RMSE of the tensor components by nearly three orders of magnitude, indicating a significant error reduction in MGT estimation accuracy. Further experimental validation confirms the practical applicability of the method: the average localization error of the magnetic source decreased from 0.040 m to 0.019 m after calibration, yielding a 52.5% improvement. These consistent improvements across both simulated and real-world settings demonstrate that the proposed calibration strategy effectively enhances the spatial resolution and localization accuracy of MGTMS.

However, the current study focuses on addresses array-level misalignment errors. The inherent sensor-level errors such as scale factor deviations and axis non-orthogonality are not considered in the current calibration framework. Future research is proposed to develop an integrated framework by incorporating joint correction of both array-level and sensor-intrinsic errors to achieve comprehensive calibration and further improve the robustness and accuracy of MGT measurements in complex environments.

#### References

- [1] Y. Zhao, J Zhang, J Li, S Liu, P Miao, Y Shi, and E Zhao, A brief review of magnetic anomaly detection. Measurement Science and Technology. **32**, 4, 042002 (2021).
- [2] X. Zheng, Y. Tian, and B. Wang, A magnetic gradient tensor based method for UXO detection on movable platform. IEEE Transactions on Geoscience and Remote Sensing. 61, 1-9 (2023).
- [3] Y. Yan, et al., An effective magnetic anomaly detection using orthonormal basis of magnetic gradient tensor invariants. IEEE Transactions on Geoscience and Remote Sensing. 62,1-11 (2024).
- [4] R. F. Wiegert, Magnetic STAR technology for real-time localization and classification of unexploded ordnance and buried mines. Proc. SPIE. **7303**, 514–522 (2009).
- [5] T. Nara and W. Ito, Moore–Penrose generalized inverse of the gradient tensor in Euler's equation for locating a magnetic dipole, J. Appl. Phys. 115, 17, 17E504 (2014).
- [6] G. Liu et al., Novel magnetic dipole localization method based on normalized source strength. IEEE Sens. J. 24, 16, 26159– 26170, (2024). 10.1109/JSEN.2024.3423342.
- [7] G. Liu, Y. Zhang, C. Wang, Q. Li, F. Li, and W. Liu, A new magnetic target localization method based on two-point magnetic gradient tensor. Remote Sens. 14, 23, 6088 (2022).

- [8] W. Chen et al., A correction method of magnetic gradient tensor system to improve magnet localization accuracy. Sens. Actuators A. 369, 115194 (2024).
- [9] X. Zhang, W. Zhang, W. Chen, and H. Zhang, A nonlinear rotation correction method for magnetic gradient tensor system. IEEE Sens. J. (2024).
- [10] Y. Mu, C. Wang, X. Zhang, and W. Xie, A novel calibration method for magnetometer array in nonuniform background field. IEEE Trans. Instrum. Meas. 68, 10, 3677–3685, (2018).
- [11] C. Chi, D. Wang, R. Tao, and Z. Yu, Error calibration of cross magnetic gradient tensor system with total least-squares method. Math. Probl. Eng. **2023**, 6974834 (2023).
- [12] C. Li and S. Zhang, Correction method of the cross-type tensor based on DA-LM. Acad. J. Sci. Technol. 5, 1, 218–225 (2023). 10.54097/ajst.v5i1.5636.
- [13] Z. Zhang, et al., Experiment research of magnetic dipole model applicability for a magnetic object. Journal of Basic Science and Engineering. 18, 5, 862-868 (2010).
- [14] F. Marini and B. Walczak, Particle swarm optimization (PSO). A tutorial Chemom. Intell. Lab. Syst. **149**, 153–165 (2015).